

This is an Open Access document downloaded from ORCA, Cardiff University's institutional repository: <https://orca.cardiff.ac.uk/id/eprint/166366/>

This is the author's version of a work that was submitted to / accepted for publication.

Citation for final published version:

Queirós-Reis, Luís, Mesquita, João R., Brancale, Andrea and Bassetto, Marcella 2023. Exploring the fatty acid binding pocket in the SARS-CoV-2 spike protein - confirmed and potential ligands. *Journal of Chemical Information and Modeling* 63 (23) , 7282–7298. 10.1021/acs.jcim.3c00803

Publishers page: <http://dx.doi.org/10.1021/acs.jcim.3c00803>

Please note:

Changes made as a result of publishing processes such as copy-editing, formatting and page numbers may not be reflected in this version. For the definitive version of this publication, please refer to the published source. You are advised to consult the publisher's version if you wish to cite this paper.

This version is being made available in accordance with publisher policies. See <http://orca.cf.ac.uk/policies.html> for usage policies. Copyright and moral rights for publications made available in ORCA are retained by the copyright holders.



Title: Exploring the fatty acid binding pocket in the SARS-CoV-2 spike protein – confirmed and potential ligands

Luís Queirós-Reis^{1}, João R. Mesquita^{1,2}, Andrea Brancale³, Marcella Bassetto^{4,5}*

1 Abel Salazar Institute of Biomedical Sciences (ICBAS), University of Porto, 4050-313
Porto, Portugal; up201205115@up.pt (L.Q.-R.)

2 Epidemiology Research Unit (EPIunit), Institute of Public Health, University of Porto,
4050-091 Porto, Portugal

3 University of Chemistry and Technology, Prague 166 28 Praha, Czechia;
andrea.brancale@vscht.cz

4 School of Pharmacy and Pharmaceutical Sciences, College of Biomedical and Life
Sciences, Cardiff University, Cardiff, CF10 3BN, UK; bassettom1@cardiff.ac.uk

5 Department of Chemistry, Faculty of Science and Engineering, Swansea University,
Swansea, SA2 8PP, UK

* Correspondence: L.Q.-R., up201205115@up.pt

Abstract

Severe Acute Respiratory syndrome 2 (SARS-CoV-2) is a respiratory virus responsible for coronavirus disease 19 (COVID-19) and the still ongoing and unprecedented global pandemic. The key viral protein for cell infection is the spike glycoprotein, a surface-exposed fusion protein, that both recognizes and mediates entry into host cells. Within the spike glycoprotein, a fatty acid binding pocket (FABP) has been confirmed, with the crystallization of linoleic acid (LA) occupying a well-defined site. Importantly, when the pocket is occupied by a fatty acid, an inactive conformation is stabilized, and cell recognition is hindered. In this review, we discuss ligands reported so far for this site, correlating their activity predicted through *in silico* studies with anti-spike experimental activity, assessed by either binding assays or cell-infection assays. LA was the first confirmed ligand, co-crystallised in a cryo-EM structure of the spike protein, resulting in increased stability of the inactive conformation of the spike protein. The next identified ligand, lifitegrast, was also experimentally confirmed as a ligand with antiviral activity, suggesting the potential for diverse chemical scaffolds with the ability to bind this site. Finally, SPC-14 was also confirmed as a ligand, although no inhibition assays were performed. In this review, we identified 20 studies describing small-molecule compounds predicted to bind the pocket in *in silico* studies, and with confirmed binding or *in vitro* activity, either inhibitory activity against the spike-ACE2 interaction, or antiviral activity in cell-based assays. When considering all ligands confirmed with *in vitro* assays, a good overall occupation of the pocket should be complemented with the ability to make direct interactions, both hydrophilic and hydrophobic, with key amino acid residues defining the pocket surface. Among the active compounds, long flexible carbon chains are recurrent, with retinoids capable of binding the FABP, although bulkier systems are also capable of affecting viral fitness. Compounds able to bind this site with high affinity have the potential to

stabilize the inactive conformation of the SARS-CoV-2 spike protein, and therefore reduce the virus ability to infect new cells. Since this pocket is conserved in all highly pathogenic human coronaviruses, including MERS-CoV and SARS-CoV, this effect could be exploited for the development of new antiviral agents, with broad-spectrum anti-coronavirus activity.

1. Introduction

1.1 SARS-CoV-2

Coronavirus disease 19, or COVID-19, is a respiratory infection caused by the Severe Acute Respiratory Syndrome Coronavirus 2 (SARS-CoV-2), responsible for a global pandemic with more than 750 million people infected and close to 7 million deaths up to September 2023 ¹⁻⁴. Coronaviruses (CoVs) are a group of RNA viruses belonging to the subfamily *Orthocoronaviridae*, that cause disease in a variety of domestic and wild animals ⁵. The name “corona” is derived from a halo observed under microscopy, formed by three major structural proteins: spike, membrane, and envelope, projecting as spikes from the viral envelope (Figure 1)⁶.

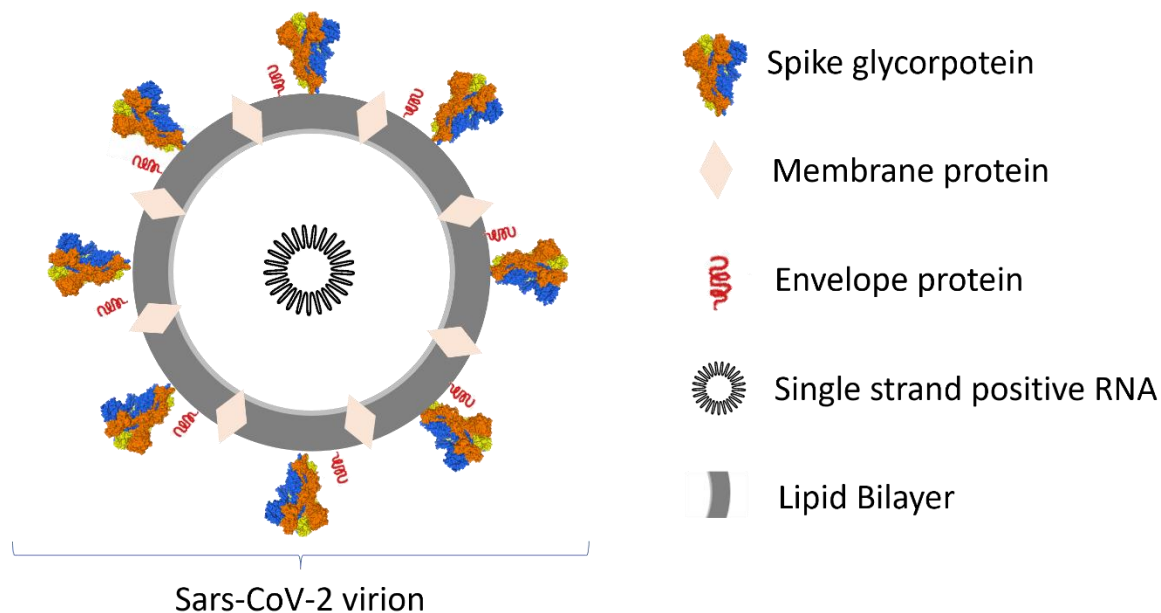


Figure 1: Schematic representation of the SARS-CoV-2 virion structure, with the single-stranded, positive-sense RNA and the three structural proteins: spike glycoprotein, membrane protein and envelope protein.

Cell infection for SARS-CoV-2 is initiated by the densely glycosylated spike (S) protein (Figure 2A), a trimeric fusion protein that binds to human angiotensin converting enzyme 2 (ACE2), acting as the functional receptor ^{1,7}. As the S protein mediates viral entry into host cells, it is the main target for antibodies and one of the primary focuses of therapeutics and vaccine design ^{8,9}. All key areas for cell and antibody recognition are located in the S protein, defining the receptor binding domain (RBD) as the portion that interacts with ACE2 (Figure 2B) ¹⁰⁻¹². Since the infection is initiated by receptor recognition between the RBD and ACE2, this interaction determines infectivity, host range and pathogenesis of the virus ⁷.

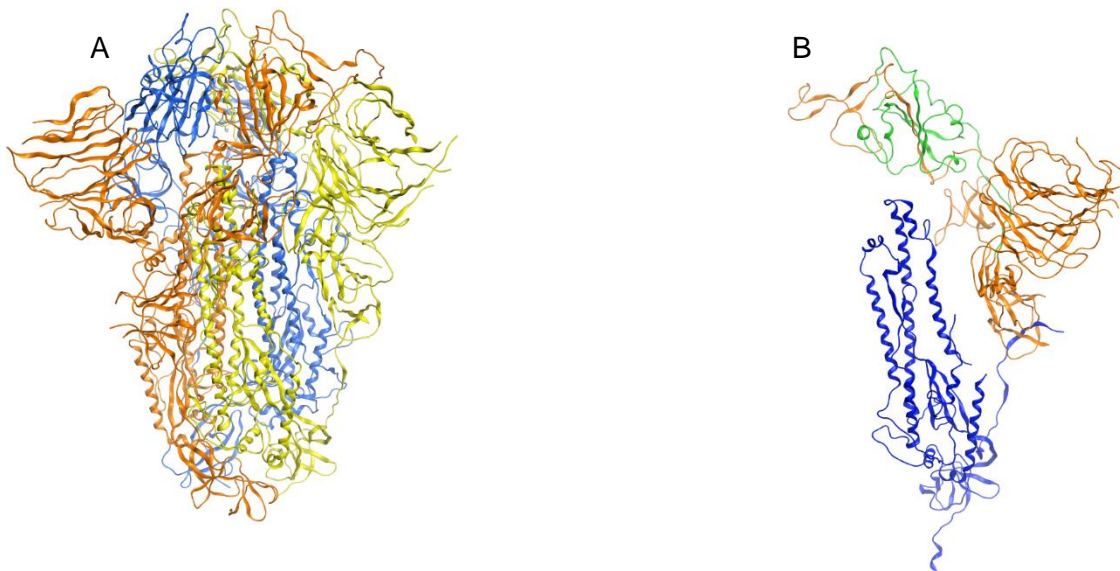


Figure 2: A) Ribbon representation of the S glycoprotein trimer, with the monomers represented as blue, orange and yellow ribbon, respectively (PDB ID: 6VXX). B) Ribbon representation of a S glycoprotein monomer with the RBD highlighted in green. The RBD is part of the S1 subunit (orange), while the S2 subunit is represented in blue ¹³.

2.2 The spike glycoprotein as a drug target

Given the critical role of the S protein, it is the main target for vaccine development, antibody therapy and small-molecule entry inhibitors ^{7, 11}. Indeed, vaccine development focused on the S protein and achieved a reduction in viral effectiveness ¹⁴. On the other hand, no small-molecule inhibitors of the S protein have been approved. When targeting the direct interaction between the RBD and ACE2, there is an intrinsic challenge, as the receptor binding motifs are highly variable at the sequence level ¹¹. Nevertheless, since it is effective in reducing viral fitness, research focusing on blocking the interaction has resulted in numerous virtual screening campaigns targeting at the S protein since the pandemic started ¹⁵⁻¹⁹. Given the S protein size (1300 residues), variety of functions (from cell recognition to cell fusion) and conformational changes, the area selected for such analyses can vary significantly, with studies focusing only on the RBD, larger portions of the S protein, and searches for additional potential binding cavities ^{18, 20-22}.

2.3 Fatty acid binding pocket

One of the hallmarks of viral infections is the imbalance they cause in regular cell functions. Specifically for coronavirus, lipid metabolism is deeply impacted and the presence of fatty acids, such as linoleic acid (LA) and arachidonic acid, can significantly suppress viral replication ²³. With this in mind, the S protein was studied in the presence of LA and a cryo-EM structure of

the S protein with LA bound was determined (PDB ID: 6ZB5), with the binding area identified as a fatty acid binding pocket (FABP). LA occupies a site formed between two adjacent RBDs, and considering that the S protein is a trimer, three similar pockets are defined, with up to three molecules of LA capable of binding simultaneously (Figure 3A) ^{24, 25}.

Critically, despite the proximity to the RBD surface that interacts with ACE2, none of the FABP residues participate in the recognition event with the human receptor ^{24, 25}. Binding to this pocket appears to be enabled by a specific spatial occupation pattern, and LA, a molecule with a long carbon chain and two cis-unsaturated bonds, appears to have an ideal molecular shape to achieve an optimal fit of the curved cavity of the pocket (Figure 3B) ²⁴.

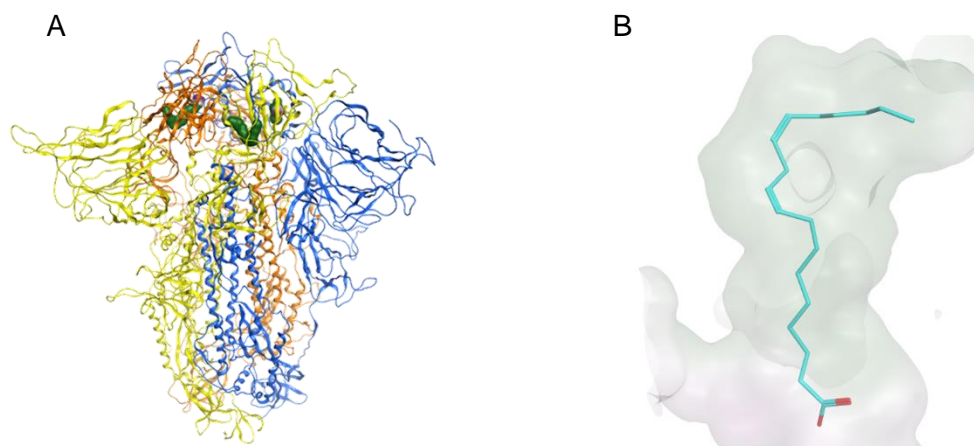


Figure 3: A) Ribbon representation of S protein from a side view, with three FABP defined near the RBD (PDB ID: 6ZB5). The S protein subunits are represented as a yellow, orange and blue ribbon, respectively, while three bound LA molecules are highlighted as molecular surface (green: lipophilic; pink: hydrophilic; white: neutral). B) Zoom on one LA molecule (carbon atoms in cyan) co-crystallized in the FABP represented by molecular surface, the hydrophilic

(purple) portion near the carboxylate group and the carbon chain buried in the hydrophobic portion (green) (PDB ID: 6ZB5) ¹³

The presence of LA in the FABP affects conformational changes in the protein elicited by the cell recognition event. Each RBD has two possible conformations: down conformation (Figure 4A), inaccessible for interaction with ACE2, or up conformation, available for target recognition (Figure 4B) ^{10, 26}. Additionally, changing between the up and down conformation is independent in each S monomer, with the down conformation being the most stable and frequent state ⁷. In the absence of LA, three-dimensional classification of S particle conformations in cryo-EM data reveals that ~70% of trimers have RBDs in the up conformation, with the S protein primed for infection. On the other hand, when LA is present, ~70% of S trimers are in an all-down conformation, incapable of binding with the ACE2 receptor ^{24, 27, 28}. The presence of LA in the FABP results in a rearrangement of the binding motifs, becoming ordered and buried between RBD interfaces, decreasing the ability of the RBD to interact with ACE2 (Figure 4A) ²⁴. The increased rigidity and stabilization of the S protein in an inactive conformation changes the ratio between up- and down-conformation RBDs ^{24, 27}.

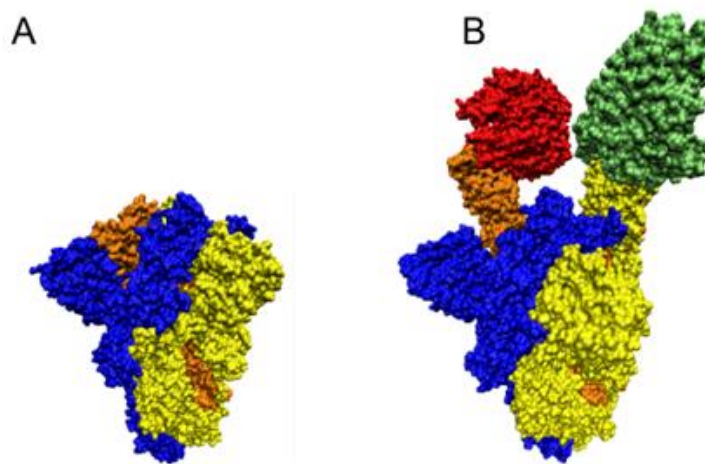


Figure 4: A) Protein surface representation of S trimer in a three RBD down conformation (blue, orange, yellow) B) Protein surface representation of S trimer in a two RBD up (yellow and orange) bound to ACE2 (red and green) and one RBD down (blue) conformation) ¹³

2.3.1 Fatty acid binding pocket - Structure

The FABP is shaped in a long, curved tube fashion, with extensive interaction surfaces formed by several phenylalanine residues (Phe338, Phe342, Phe374, Phe377, Phe392, Phe515), as well as other mainly hydrophobic amino acids (Cys336, Pro337, Ile358, Ala363, Tyr365, Leu368, Tyr369, Leu387, Val395, Ile434, Leu513, Val524) ^{24, 25}. At the entrance of the pocket, the adjacent RBD provides several hydrophilic residues that can establish both electrostatic and hydrogen-bond interactions (Arg408, Gln409, Gly416, Lys417) ^{24, 25}. Potential ligands can interact with residues in both portions and the presence of the adjacent RBD is required to stabilize the ligand by forming direct interactions with the hydrophilic groups ^{24, 29}. Regarding LA, the main stabilizing interactions are a hydrogen bond between Lys417 and the carboxylic acid from LA, and additional contacts across the pocket with Phe338, Tyr365 and Cys432 (Figure 5) ²⁴.

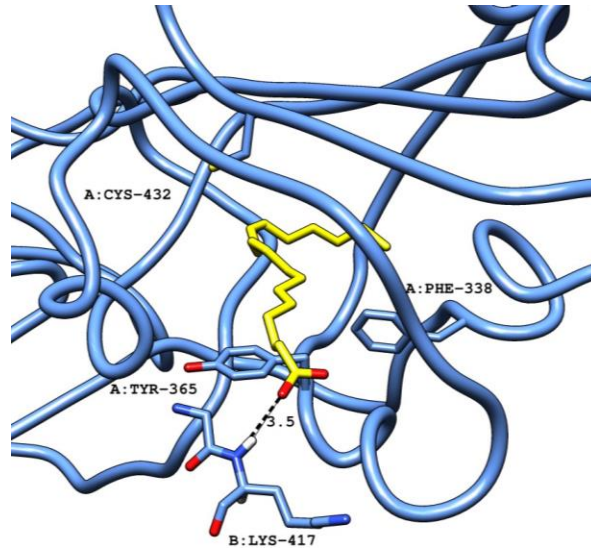


Figure 5: A) Crystallized LA ((PDB ID: 6ZB5) (carbon atoms in yellow) in the FABP in ribbon representation (blue), located between two adjacent RBDs. The pocket is formed by RBD-A (with hydrophobic residues) and hydrophilic residues in the adjacent RBD-B, interacting with the carboxylate head. Black dashed lines represent polar interactions (hydrogen bonds and electrostatic interactions) between the ligand and amino acid residues in the protein.

2.4 Occupation of the fatty acid binding pocket and viral infection

LA, as other similar ω -6 fatty acids, can affect virus binding to ACE2 and cell entry, and its increased intake has been linked to decreased fatality rates in epidemiological studies³⁰⁻³². A direct inhibitory effect in the RBD-ACE2 interaction has been detected, with a 18% reduction in binding assays at 0.29 mM, while linolenic acid displays a reduction of up to 60% infection in cell-based assays at 2.28 mM, which confirms the potential to modulate the S activity from this pocket³⁰. The presence of fatty acids in the FABP, particularly LA, affects conformational rearrangements, infectivity and immunogenicity²⁹. In addition to the direct effects in recognition from the stabilization of the RBDs, there is also the potential for distal effects in the S protein,

modulating the behaviour of key residues involved in major conformational rearrangements preceding cell fusion ³³. Computational studies exploring the pH-dependence of S protein conformations, based upon pKa calculations and molecular dynamics simulations at constant pH, have suggested that LA binding affects the pH-dependence of the RBD active/inactive conformation equilibrium ³⁴. The FABP is located in the vicinity of the base pair Asp398-Arg355, and the decreased flexibility upon fatty acid binding changes the solvent accessibility of Arg355, since the regions adjacent to both amino acids are more closely packed, with a similar effect also observed for Asp614 (Figure 6) ³⁴. The observed effect in Asp614 is particularly relevant, taking into account that a mutation in this residue is now prevalent in all circulating SARS-CoV-2 variants (Asp614Gly), increasing infectivity by reducing interactions within the S protein, and shifting the protein conformation towards active RBDs ^{28, 34, 35}. LA has the opposite effect on the conformational states of the S protein, affecting the pH-dependence and shifting the protein conformation towards inactive RBDs ^{10, 36}.

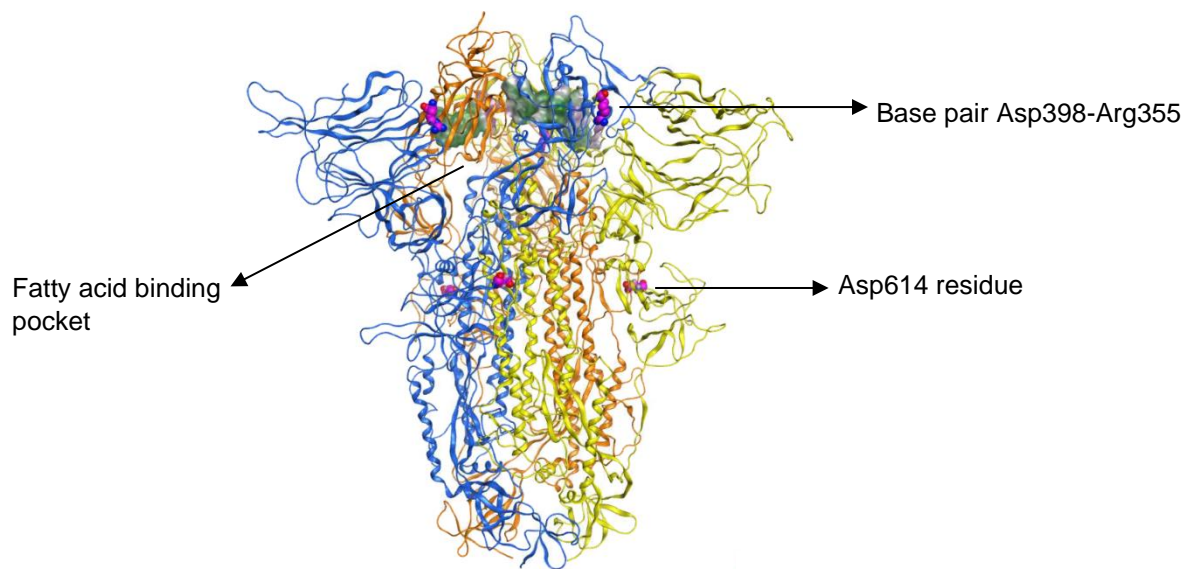


Figure 6: Ribbon representation of the S trimer (PDB ID: 6ZB5), in side view with the base pair Asp398-Arg355 and residue Asp614 represented with carbon atoms in purple. The FABP is represented as a molecular surface ¹³.

In addition to a strong effect in the S trimer behaviour and target recognition abilities, exploring the potential occupation of the FABP with small-molecule ligands presents an additional advantage, given that key residues in the pocket are highly conserved, not only among emerging SARS-CoV-2 variants of concern, but also in intermediate species, such as coronaviruses currently infecting bats and pangolins ^{25, 29, 37}. Whilst the pH-dependence of the S protein is highly relevant for the virus life cycle, particularly during the endosomal pathway for cell entry, the function of the FABP is not clear, although a modulation effect in the exposure of immunodominant sites has been suggested ^{29, 36}. During endosomal entry, as the environmental pH is gradually reduced, the open/closed RBD equilibrium is shifted to the inactive conformation, reducing not only the interaction with ACE2, but also with neutralizing antibodies, that commonly bind the RBD ³⁶. As a result, neutralizing antibodies are shed gradually, but partial interaction with ACE2 is maintained, along with the ability for cell fusion and infection ^{36, 38}. This has been described as a masking behaviour, where all RBDs are in the inactive conformation ³⁶. Similarly, the presence of LA also stabilizes the inactive conformation, in a masking behaviour, restricting viral replication ²⁹. As happens for a decreasing pH, the FABP appears to be essential for effective infection, allowing the virus to change from a high-infective status before a host immune response is established, with subsequent inflammation producing ω -3 and ω -6 molecules that activate the FABP, reducing viral recognition and clearance, while increasing viral titers ²⁹. Hence, the FABP modulates conformational changes

that affect the immunogenicity of the S protein ²⁹. Taking into account the confirmed binding effect of ω -6 fatty acids, which decrease target recognition and viral replication ³⁰, the FABP is a promising target for the development of small-molecule binders, that could lock the S trimer and respective RBDs in an inactive conformation, inhibiting receptor interactions and cell infection ^{1, 8, 24}. This is particularly important, as this binding pocket is not exclusive to SARS-CoV-2: it is found in other highly infectious human coronaviruses, being fully conserved in SARS-CoV, and partially conserved in MERS-CoV. This pocket could therefore be exploited for the development of new antiviral agents with broad-spectrum anti-coronavirus activity ²⁵.

The main objective of this article is to compile currently confirmed and potential ligands, resulting from virtual screening studies that explore the FABP, either focusing on the pocket specifically, or broader virtual screenings against the whole S glycoprotein. Given the potential to significantly affect the virus life cycle by binding to the FABP, a comprehensive understanding of which ligands are known to bind to this site, and their inhibitory activity of the S-ACE2 interaction and/or cell infection, may support the development of novel, potentially broad-spectrum, therapeutic agents. Furthermore, a systematic elucidation of how each confirmed ligand binds, highlighting favoured functional groups and scaffolds, and essential interactions, can aid the design of new molecules with improved binding to this site, which may help in the inhibition of coronavirus infections. Compounds with potential or confirmed activity were evaluated with molecular docking analyses in the FABP when this data was unavailable, to aid the discussion of potential interaction patterns.

3 Methods

3.1 Literature review

The systematic review followed the Preferred Reporting of Systematic Reviews and Metanalysis (PRISMA) ³⁹. We concluded an extensive search for virtual screening studies focusing on the S protein through different databases, namely MEDLINE (PubMed), Scopus and Web of Science®, to select literature published until May 15th, 2022. The main goal was to find compounds predicted to bind the FABP and, as such, we collected all articles containing (“SARS-CoV-2” + “spike” + “virtual screening”) in the title or abstract. Additionally, since LA, a fatty acid, is a known ligand, we also collected articles with the terms (“SARS-CoV-2” + “spike” + “linoleic acid”) and (“SARS-CoV-2” + “spike” + “fatty acid”). As summarised in the PRISMA Diagram (Supporting Information Figure S1), a total of 738 articles were identified; filtering for duplicate articles resulted in a total of 387 different articles. From these, 159 articles were excluded since they were not virtual screening studies or had no experimental data regarding the S1 subunit or binding to the FABP. Finally, an additional 208 articles were also excluded, since they were either virtual screening studies focusing exclusively on the S-ACE2 interaction, or they reported no compounds predicted to interact with any FABP residues. Additional articles were added with complementary information, such as binding inhibition or cell-based assays. From the final selection of 20 articles, 21 compounds were identified with predicted binding to the S glycoprotein, along with complementary experimental results confirming either binding or functional activity. Additionally, 6 compounds were identified as possible binders, although no experimental assays were available. Identified structures with confirmed activity or potential activity were analysed with docking simulations to further explore potential interactions.

Docking Simulations

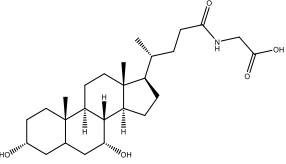
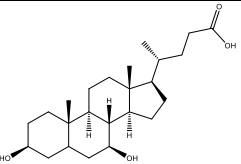
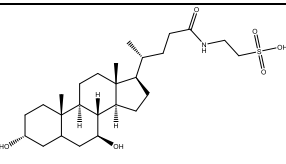
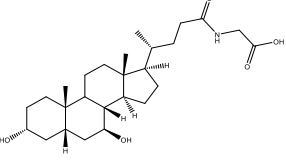
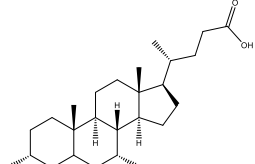
All molecular modelling experiments were performed on an Asus WS X299 PRO Intel® i9-10980XE CPU @ 3.00 GHz × 36 running Ubuntu 18.04 (graphic card: GeForce RTX 2080 Ti). Molecular Operating Environment (MOE) 2019.10¹³ and Maestro (Schrödinger Release 2020-2) were used as molecular modelling software⁴⁰. The structures of the compounds analysed were built in MOE, saved in .sdf format, and prepared using Maestro LigPrep tool by energy minimizing the structures (OPLS_2005 force field), generating possible ionization states at pH 7 ± 2, tautomers, all possible stereoisomers per ligand and low-energy ring conformers. The crystal structure of LA in the S glycoprotein was downloaded from the PDB (<http://www.rcsb.org/> (accessed on 15 May 2023); PDB code 6ZB5). The protein was pre-processed with MOE Protein Preparation tool, the resulting protein-ligand complex was saved in .mae format and prepared using Schrödinger Protein Preparation Wizard by assigning bond orders, adding hydrogens, and performing a restrained energy minimization of the added hydrogens using the OPLS_2005 force field. A 15 Å docking grid was prepared using the co-crystallized LA as the centroid. Molecular docking studies were performed using Glide SP, keeping the default parameters, and setting 5 as the number of output poses per input ligand, performing for each pose a post-docking minimization. The output poses were saved as mol2 files. The docking results were visually inspected using MOE 2019.10.

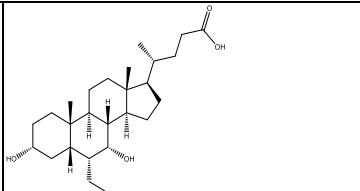
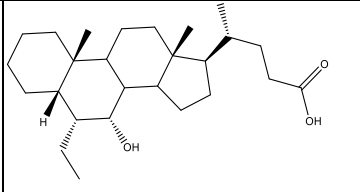
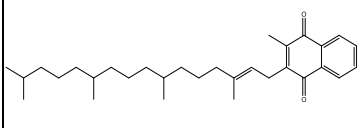
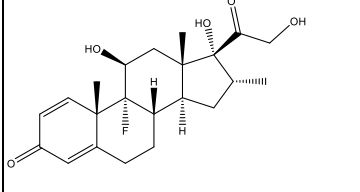
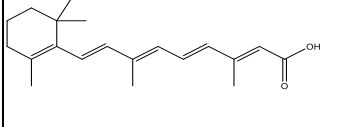
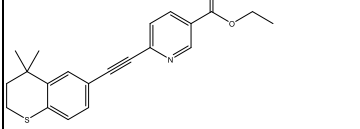
4 Results

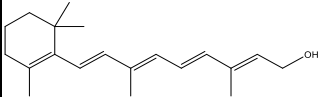
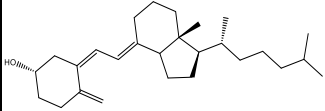
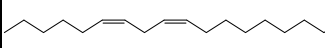
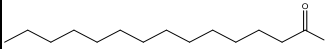
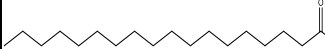
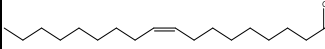
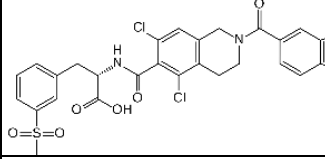
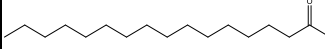
4.1 Compounds interacting with the FABP

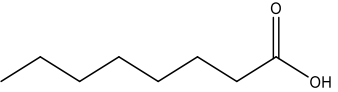
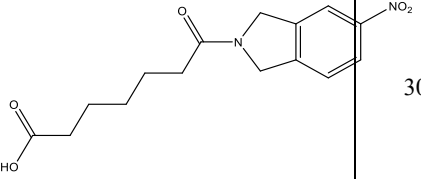
Predicted interactions with the FABP for selected compounds are reported in virtual screening studies, however experimental confirmation of binding and its effect in receptor recognition/cell entry is not always available. Therefore, compounds with reported experimental data were prioritized (Table 1), with additional compounds identified when only predicted interactions are available (Table 2). The libraries from which these compounds are derived vary widely, from studies testing a single compound, to libraries of a few thousand molecules. Selected compounds may originate from libraries with plant metabolites or other biological sources ⁴¹. Identification of compounds potentially active in the FABP was based on described interactions, either predicted, in virtual screening studies, or directly confirmed, by cryo-EM or NMR experiments. Regarding experimental validation, data was crossed with additional studies, whenever complementary information was available. It should be noted that, when direct FABP activity is not accessed, validation was based on inhibition assays for the S-ACE2 interaction or cell-based infection assays, without, however, confirming specific interaction in the FABP. Finally, the selection of compounds without experimental validation (Table 2) was based on the patterns of interaction identified for LA, focusing on residues that compose the FABP.

1 Table 1 - Confirmed and potential ligands of the FABP, with *in silico* studies and complementing *in vitro* testing

Compound	Structure	Molecular weight	cLogP ^a	LogD ^b (pH=7)	<i>In silico</i> studies	<i>In vitro</i> studies	Reference
Glyco-chenodeoxycholic acid		449.6	3.05	-0.5	Binding pocket: Fpocket webserver with PDB ID: 6VSB Docking software: AutoDock	~ 15 % reduction in S-AI ^c in binding assays at 10 µM	42
Ursodeoxycholic acid		392.57	3.60	0.4	Binding pocket: Fpocket webserver with PDB ID: 6VSB Docking software: AutoDock	~ 15 % reduction in S-AI ^c in binding assays at 10 µM	42
Tauro-ursodeoxycholic acid		499.7	2.76	-0.2	Binding pocket: Fpocket webserver with PDB ID: 6VSB Docking software: AutoDock	~ 5 % reduction in S-AI ^c in binding assays at 10 µM	42
Glyco-ursodeoxycholic acid		449.6	3.05	-0.5	Binding pocket: Fpocket webserver with PDB ID: 6VSB Docking software: AutoDock	~ 20 % reduction in S-AI ^c in binding assays at 10 µM	42
Chenodeoxycholic acid		392.6	3.60	1.3	Binding pocket: Fpocket webserver with PDB ID: 6VSB Docking software: AutoDock	~ 10 % reduction in S-AI ^c in binding assays at 10 µM	42

Obeticholic acid		420.6	4.16	2.1	Binding pocket: Fpocket webserver with PDB ID: 6VSB Docking software: AutoDock	~ 15 % reduction in S-AI ^c in binding assays at 10 μ M	42
BAR 704		392.62	4.46	4.1	Binding pocket: Fpocket webserver with PDB ID: 6VSB Docking software: AutoDock	~ 35 % reduction in S-AI ^c in binding assays at 10 μ M	42
Vitamin K		450.7	8.34	9.7	Binding pocket: LA in PDB ID: 6ZB5 Docking software: BUDE docking server	50% reduction in virion retention in cells at 4.7 μ M	19, 29
Dexamethasone		392.5	2.14	1.7	Binding pocket: LA in PDB ID: 6ZB5 Docking software: BUDE docking server	50 % reduction in virion retention in cells at 3.2 μ M	19, 29
Tretinoin		300.4	5.01	3.0	Binding pocket: LA in PDB ID: 6ZB5 Docking software: BUDE docking server	~ 60 % reduction in viral replication in cells at 1 μ M	19, 43
Tazarotene		351.5	4.61	5.2	Binding pocket: LA in PDB ID: 6ZB5 Docking software: BUDE docking server	~ 50 % reduction in viral replication in cells at 1 μ M	19, 43

Vitamin A		286.5	5.04	4.7	Binding pocket: LA in PDB ID: 6ZB5 Docking software: BUDE docking server	100% reduction in S-AI ^c in binding assays at 2.5 μ M	19, 30
Vitamin D3		384.6	6.85	7.1	Binding pocket from: LA in PDB ID: 6ZB5 Docking software: BUDE docking server	15% reduction in S-AI ^c in binding assays at 2.5 μ M	19, 30
Linoleic acid		280.4	5.45	4.4	Binding pocket: LA in PDB ID: 6ZB5 Docking software: BUDE docking server	100% reduction in S-AI ^c in binding assays at 2.5 μ M	24, 30
Myristic acid		228.4	4.45	3.3	Binding pocket: FABP in 6VXX Docking software: Glide XP	15% reduction in S-AI ^c in binding assays at 2.5 μ M	30, 44
Stearic acid		284.5	5.93	5.1	Binding pocket: FABP in 6VXX Docking software: Glide XP	20% reduction in S-AI ^c in binding assays at 2.5 μ M	30, 44
Oleic acid		282.5	5.71	4.8	Binding pocket: FABP in 6VXX Docking software: Glide XP	90% reduction in S-AI ^c in binding assays at 2.5 μ M	30, 44
Lifitegrast		615.5	4.19	1.2	Binding pocket: S-ACE2 interaction surface in PDB ID: 6VW1 Docking software: Autodock Vina	50% reduction in cell infection at 1,295 μ M	45, 46
Palmitic acid		256.5	5.20	4.2	Binding pocket: FABP in PDB ID 6VXX Docking software: Glide SP, Glide XP	15% reduction in S-AI ^c in binding assays at 2.5 μ M	30, 44

Caprylic acid		144.2	2.23	0.9	Binding pocket: FABP in PDB ID 6VXX Docking software: Glide SP, Glide XP	20% reduction in S-AI ^c in binding assays at 2.5 μ M	30, 44
SPC-14		306.3	1.29	-0.7	Binding Pocket: FABP in PDB ID 7E7B Docking software: DOCK3.7	Binding confirmed in SPR and cryo-EM No inhibition or cell-based assays	47

2 ^a Calculated with SwissADME ⁴⁸

3 ^b Calculated using Chemaxon® LogD calculator ⁴⁹

4 ^c S-AI S-ACE2 interaction

As with LA, most compounds in Table 1 have a molecular weight over 250 and below 500 g/mol, likely required to adequately occupy the pocket. Despite the FABP being composed mainly of hydrophobic amino acids, the predicted logP of confirmed ligands varies between 1 and 8, whilst predicted logD (pH=7) varies between -0.5 and 9.7. These variations are due to the presence of functional groups (such as carboxylic acids and hydroxy groups) capable of interacting with positively charged amino acid residues. Another significant feature is the overall rigidity of the scaffold: while LA, the first confirmed ligand for this pocket, is flexible, this does not appear to be an essential requirement, as confirmed by lifitegrast, characterized by bulkier and rigid ring systems. As expected from the Cryo-EM structure with LA (PDB ID: 6ZB5), the predicted binding for these compounds always features two RBDs, and interactions with both the hydrophilic and hydrophobic portions of the pocket.

4.2 Confirmed ligands of the FABP

Despite the experimental effect in the virus-host interaction detected for multiple compounds, only two have been confirmed to directly bind the FABP and exert a biological activity, lifitegrast and LA^{24, 46}. Lifitegrast is a drug (Xiidra®) used for the treatment of dry eye disease as an ophthalmic solution⁵⁰, and while LA has been co-crystallized in the S protein, lifitegrast was identified in a virtual screening study, for its predicted direct inhibition of the S-ACE2 interaction, unrelated to the FABP⁴⁶. Lifitegrast predicted activity was confirmed later, as it was found to significantly reduce the S-ACE2 interaction in surface plasmon resonance (SPR) analyses⁴⁶. Remarkably, additional studies have pointed to an effect through the FABP: measured with chemical shift perturbation (CSP) NMR, the chemical perturbation of lifitegrast matches the effect of LA, suggesting an action on the FABP instead of the protein surface⁴⁵. Furthermore, saturation transfer difference (STD) NMR showed that all aromatic groups of lifitegrast are in contact with the RBD and buried in

the FABP, as would be expected for binding to the hydrophobic portion of the pocket ⁴⁵.

Binding assays determined a K_D of 1.92 nM with the S protein for lifitegrast, and a reduction of 99.8% of the RBD-ACE2 protein-protein interaction in SPR competition assays at 1.92 nM ⁴⁶. Consequently, further cell-infection studies determined an IC_{50} of 1,295.3 μ M for *in vitro* infection of Vero E6 cells with no cytotoxicity up to 5 mM ⁴⁶. Given that lifitegrast was identified when screened against the RBD but its activity was later reconducted to binding in the FABP, we performed a docking analysis in the FABP with Glide SP ⁴⁰, to predict how it may bind the FABP (Figure 7) ⁵¹.

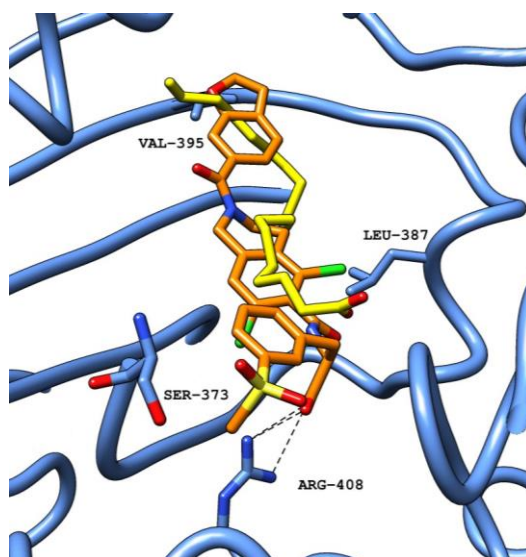


Figure 7: Crystalized LA (PDB ID: 6ZB5) (carbon atoms in yellow) superimposed with lifitegrast (carbons atoms in orange) in the FABP in ribbon representation (blue). Dashed lines represent polar interactions (hydrogen bonds and electrostatic interactions) between the ligand and amino acid residues in the protein ⁵².

In line with the network of interactions with hydrophobic moieties detected in NMR assays, lifitegrast can be deeply buried in the hydrophobic region of the pocket ⁴⁵. As with LA, the predicted pose found for lifitegrast can be stabilized by interaction with hydrophilic residues (Arg408), and additional contacts with the hydrophobic amino acids (Ala372, Ser373,

Leu387 and Val395). Additionally, the predicted binding pose for lifitegrast indicates an extensive pocket occupation. Taken together, LA and lifitegrast show that although molecules with long and flexible carbon chains can access the pocket and influence cell infection and the virus life cycle, more rigid and bulkier compounds can also adequately bind and exert an effect through occupation of the FABP. In addition to lifitegrast and LA, SPC-14 has also been confirmed to bind the FABP, although no inhibition assays on the interaction between the S protein and ACE2 have been reported ⁴⁷. Binding was determined in SPR assays with the S protein, resulting in a binding affinity (KD) of 9.5 μ M, with further cryo-EM structural determination confirming binding and clarifying how this compound binds to the FABP (Figure 8) ⁴⁷.

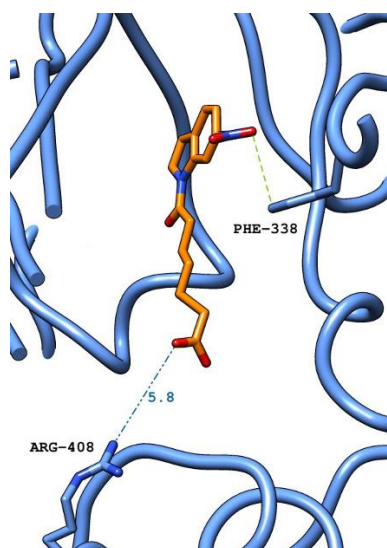


Figure 8: Crystallized SPC-14 (carbon atoms in orange) (PDB ID:8H3E) in the FABP in ribbon representation (blue). Green dashed line represents hydrophobic interactions and blue dashed line represents the distance between SPC-14 and the sidechain of Arg408 ⁵².

The cryo-EM structure for SPC-14 shows a different interaction pattern to LA, as SPC-14 is further buried in the pocket, and hydrophobic stabilizing interactions are prominent, particularly with the nitro group having π -stacking interaction with Phe338⁴⁷. Although no interactions are directly established with the hydrophilic portion of the site, the carboxylic acid remains at a distance of 6 Å from the hydrophilic residue Arg408 (Figure 8). Along with the co-crystallization of SPC-14, 48% of S protein population appeared in the closed conformation, with the remaining only showing one RBD exposed for interaction with ACE2⁴⁷. The data collected for SPC-14 suggests that it is likely to affect the RBD-ACE2 interaction, and potentially the virus life cycle, although this has not yet been confirmed experimentally.

4.3 Compounds with predicted binding and confirmed activity

4.3.1 Sterol backbone

Although LA and lifitegrast have been explicitly confirmed to bind the FABP and have experimental results for their direct binding to the FABP, leading to reduced interaction or cell infection, other compounds with exclusively binding or cell-based assays could potentially act through binding the FABP. In a virtual screening campaign, natural bile acids and semi-synthetic derivatives were predicted to establish interactions in a proposed pocket, with common residues to the FABP, defined with the Fpocket online tool (using the S protein PDB ID 6VSB)^{42, 53}. Proposed interactions are established with residues Lys378, Thr376, Phe377, Cys379, Tyr380 and Pro384, suggesting that the molecules selected could interact with FABP residues⁴². Importantly, activity was confirmed for these compounds in S-ACE2 inhibitor screening assays, with the best ligand, BAR704, reaching up to 40% inhibition at a 10 μ M concentration⁴². However, interaction with the FABP is not discussed, as some activity is detected, and in order to predict if BAR704 could interact with this pocket, we

performed a docking analysis with Glide SP, obtaining the predicted binding pose illustrated in Figure 9 ⁵¹.

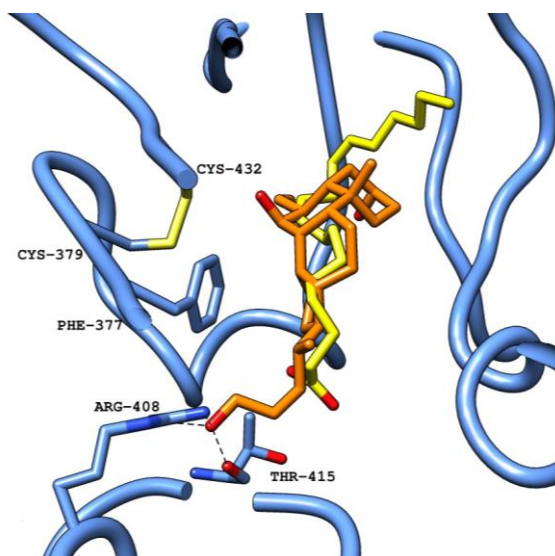


Figure 9: Crystallized LA (PDB ID: 6ZB5) (carbon atoms in yellow) superimposed with BAR 704 (carbons atoms in orange) in the FABP in ribbon representation (blue). Black dashed lines represent polar interactions (hydrogen bonds and electrostatic interactions) between the ligand and amino acid residues in the protein ⁵².

Bar704 is predicted to achieve a good overall occupation of the pocket and potentially establish interactions with residues Cys379, Cys432, Arg408, Thr415, and Phe377. Predicted interactions with Arg408, Phe377 and Cys432 are in common with LA ²⁴. Since, similarly to lifitegrast, this bile acid derivative possesses a bulkier scaffold, it can be expected to have the same ability to enter the pocket and potentially influence the virus-host interaction, resulting in the reduced S-ACE2 interaction observed.

In addition to bile acids, further compounds with a steroid backbone have been identified in molecular dynamics studies, namely dexamethasone, with an irregular interacting pattern ¹⁹. Dexamethasone's activity has been confirmed in experimental assays against the S protein, in which it reduced S-mediated binding to the ACE2 receptor, with an IC₅₀ of 3.2 μ M for

retention of virions in A549 human alveolar basal epithelial cells ²⁹. A docking analysis using Glide SP has generated the predicted binding pose shown in Figure 10. The irregular predicted pattern (hydrophobic interaction with Phe377) of interaction suggests that dexamethasone is buried in the pocket, perhaps with a pattern similar to SPC-14 and no direct interaction with the hydrophilic region ^{19, 47}.

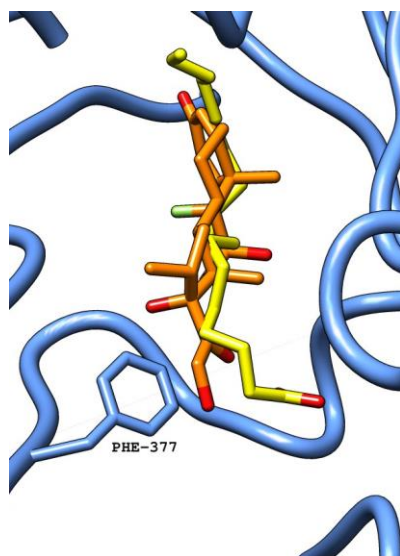


Figure 10: Crystalized LA (PDB ID: 6ZB5) (carbon atoms in yellow) superimposed with dexamethasone (carbons atoms in orange) in the FABP in ribbon representation (blue). Black dashed lines represent polar interactions (hydrogen bonds and electrostatic interactions) between the ligand and amino acid residues in the protein ⁵².

4.3.2 Fatty acids

In addition to LA, other fatty acids are also expected to bind the FABP and affect the RBD-ACE2 interaction, with non-saturated, mono and poly-unsaturated fatty acids included in virtual screening campaigns against the pocket and predicted to interact similarly to LA ⁴⁴. Palmitic acid, a saturated fatty acid, has been described as a potential ligand ⁴⁴. However, experimental results disprove this, possibly due to the bent nature of the pocket, with the cis-bonds present in LA appearing to favour an optimal binding. Palmitic acid is associated with a modest 15% reduction in S-ACE2 binding assays at 9.8 mM and no direct binding to the S protein identified, when monitored with liquid chromatography–mass spectrometry. On the other hand, oleic acid and LA were both detected bound to the S glycoprotein ^{29, 30, 38}. This is further extended to other saturated fatty acids, with myristic and stearic acid resulting in 15% and 10% reduction in binding assays at 10.9 mM and 8.8 mM, respectively ^{29, 30}. Multiple polyunsaturated fatty acids have shown a 100% reduction in binding assays at ~ 8 mM, such as linolenic acid (9.0 mM), eicosapentaenoic acid (8.3 mM) and LA (8.9 mM), consistent with predicted binding poses ³⁰. As for monounsaturated fatty acids, these show varying behaviours in between polyunsaturated and saturated, with oleic acid achieving a strong effect at relatively high concentrations (90% reduction in binding assays at 8.9 mM) and palmitoleic acid producing instead a weak effect (10 % reduction in binding assays at 9.8 mM). (Figure 11) ^{29, 30}. For polyunsaturated fatty acids, as multiple double bonds are present, the molecule is able to accommodate and appropriately fit in the pocket, in contrast with the effect in activity for monounsaturated fatty acids, where oleic acid and palmitoleic acid show widely different activity ^{29, 30}. This may be attributed to the unsaturated bond, with oleic acid being an ω -9 fatty acid and palmitoleic an ω -7, with the extended carbon chain after the double bond likely leading to different pocket occupation and establishing different interactions.

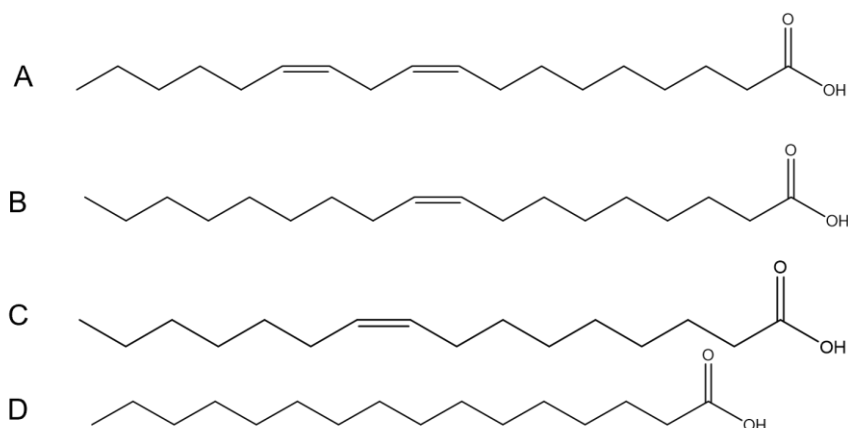


Figure 11 – A) Structures of (A) LA (polyunsaturated), (B) oleic acid (ω -9), (C) palmitoleic acid (ω -7) and Palmitic acid (unsaturated).

4.3.3 Retinoids and lipid-soluble vitamins

As with fatty acids, lipid soluble vitamins (A, D and K), as well as tazarotene and tretinoin could be good ligands for the FABP, identified in virtual screening studies¹⁹. Inhibitory activity has been confirmed for vitamins A and K, with vitamin A successfully blocking the interaction with ACE2 (100% reduction in S-ACE2 binding assays at 8.7 mM), whilst vitamin D only reduced the interaction in S-ACE2 binding assays by 13% when tested at 6.0 mM³⁰. Additional experimental assays for vitamin K showed S-mediated reduction of binding to ACE2, with an IC₅₀ of 4.7 μ M for retention of virions in A549 human alveolar basal epithelial cells [20]. To further elucidate the interaction with the FABP, we have generated a binding pose with a docking simulation using Glide SP (Figure 12)⁵¹.

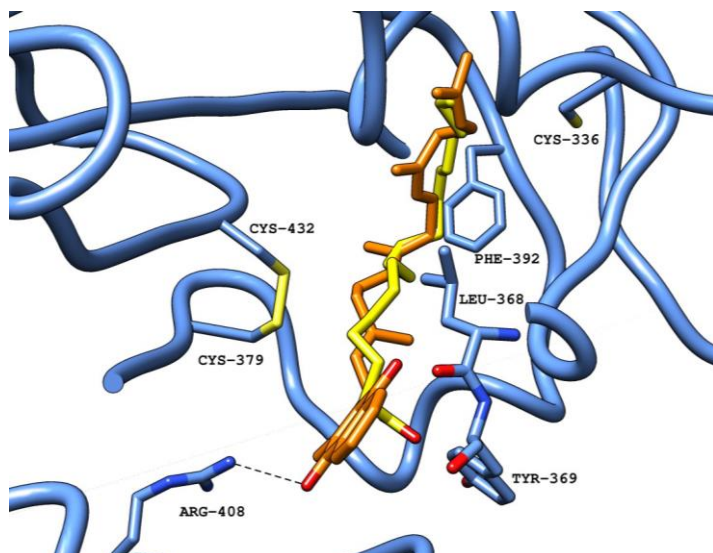


Figure 12: Crystallized LA (PDB ID: 6ZB5) (carbon atoms in yellow) superimposed with vitamin K (carbon atoms in orange) in the FABP in ribbon representation (blue). Black dashed lines represent polar interactions (hydrogen bonds and electrostatic interactions) between the ligand and amino acid residues in the protein ⁵².

Vitamin K is predicted to occupy the pocket similarly to LA, establishing polar interactions with residue Arg408 ¹⁹. In the generated pose, additional contacts with residues Leu368 and Tyr369 are predicted, and the long flexible chain extends deep into the hydrophobic portion of the pocket and establishes further interactions with residues Cys336, Cys379, Phe392 and Cys432. The predicted extensive network of interactions justifies the stabilization within the pocket and the ability to affect the virus-host interaction, with antiviral activity detected in virion cell infection assays ^{19,29}. Vitamin D is also predicted to bind to the FABP, although S-ACE2 binding assays show limited binding (13% reduction at 6.5mM) ^{19,30}. Predicted interactions are similar to LA, with direct contacts with Arg408 and Gln409 identified through molecular dynamics simulations ¹⁹. The best binding pose generated by Glide SP for vitamin D (Figure 13) ⁵¹ is in line with this observation, both for the main stabilizing interactions and the overall pocket occupation ¹⁹. Other molecular properties, such as molecular weight (Vit D: 384.6 g/mol; LA: 280.4 g/mol), predicted log P values (Vit D: 6.85;

LA: 5.45) or predicted LogD at pH=7 (Vit D:7.1; LA:4.4) could point to an increase of hydrophobic features, reflected in these values, as a potential trend in support of decreased binding. However, vitamin K surpasses vitamin D in all parameters (MW: 444.65g/mol, LogP:7.66,LogD:9.7), but maintains both binding and FABP-mediated functional effect ²⁹.

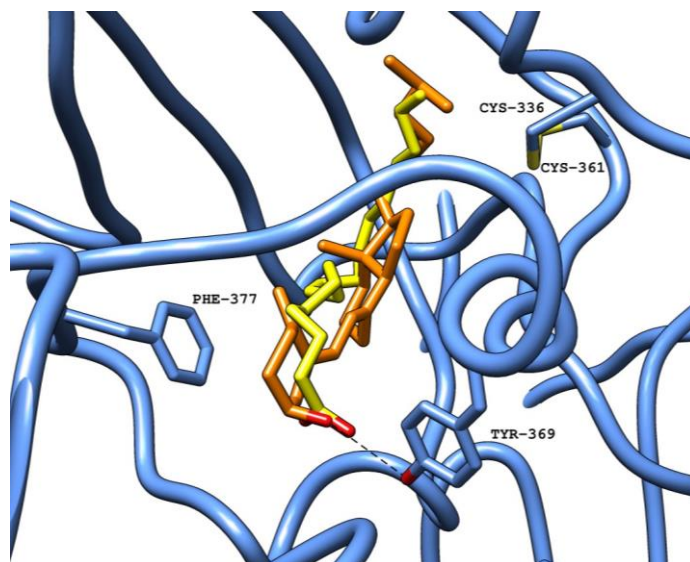


Figure 13: Crystallized LA (PDB ID: 6ZB5) (carbon atoms in yellow) superimposed with vitamin D (carbons atoms in orange) in the FABP in ribbon representation (blue). Black dashed lines represent polar interactions (hydrogen bonds and electrostatic interactions) between the ligand and amino acid residues in the protein ⁵².

4.3.4 Retinoids

Given that vitamin A has been confirmed to bind the FABP and to affect the S-ACE2 interaction, additional retinoids could be expected to have a similar effect. Particularly, tretinoin and tazarotene have been identified in both virtual screening studies and high-throughput screening studies, with predicted binding in the FABP and reduced viral infection by ~50% in Vero E6 cells at a test concentration of 1 μ M for both compounds ^{19, 43}. Taking into account the structural features of previously identified compounds binding the FABP, these retinoids are expected to bind strongly to the pocket.

Virtual screening studies predicted a polar interaction with Arg408 for these retinoids, anchoring the molecules in the pocket, an essential feature previously described for LA ¹⁹. Additional binding poses generated with Glide SP ⁵¹, have, for vitamin A (Figure 14A), the hydroxyl group in direct contact Thr415, whereas Tazarotene (Figure 14C) is predicted to interact with Tyr369. On the other hand, in the hydrophobic portion of the pocket, all three compounds are predicted to establish π -stacking or hydrophobic interactions with phenylalanine residues (Phe492 for vitamin A and tazarotene, Phe515 for tretinoin (Figure 14B) or Cys336 (for tretinoin), with a predicted pocket occupation similar to LA.

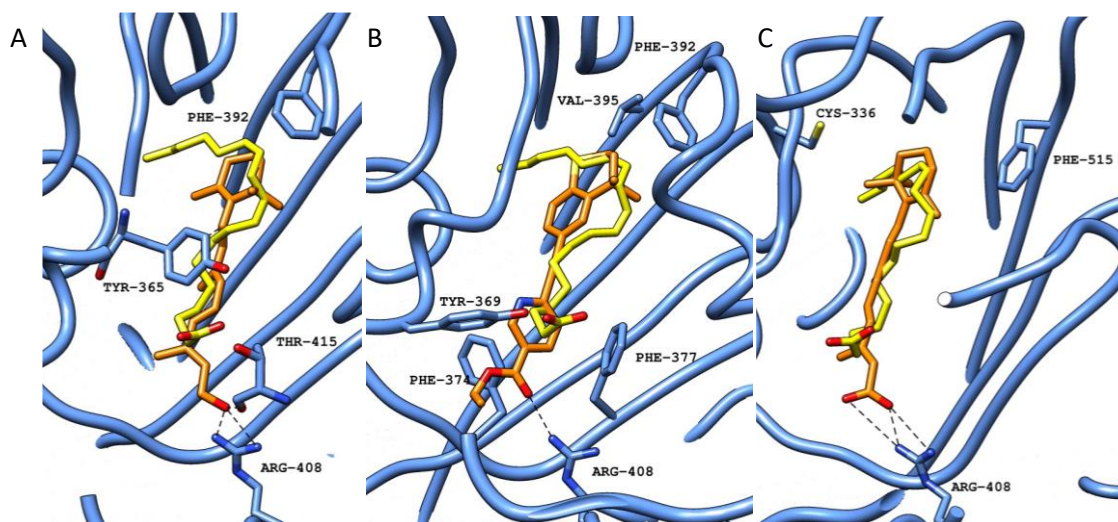


Figure 14: A) Crystallized LA (PDB ID:6ZB5) (carbon atoms in yellow) superimposed with the predicted binding pose for vitamin A (carbon atoms in orange) in the FABP in ribbon representation (blue). B) Crystallized LA (PDB ID:6ZB5) (carbon atoms in yellow) superimposed with the predicted binding pose for tazarotene (carbon atoms in orange) in the FABP in ribbon representation (blue). C) Crystallized LA (PDB ID:6ZB5) (carbon atoms in yellow) superimposed with the predicted binding pose for Tretinoin (carbon atoms in orange) in the FABP in ribbon representation (blue). Black dashed lines represent polar interactions (hydrogen bonds and electrostatic interactions) between the ligand and amino acid residues in the protein ⁵².

To summarize, the compounds discussed so far have shown the ability to bind the FABP, confirmed for LA, lifitegrast and SPC-14, and/or to affect the S-ACE2 interaction in binding assays, consequently resulting in reduced cell infection detected in cell-based assays. Binding trends include the ability to interact with hydrophobic residues buried in the pocket, and with polar functional groups of amino acid residues that define the pocket entrance. Additionally, there are two main structural features in the chemical scaffold of active compounds. The first is the presence of bulky ring-based systems, as happens with lifitegrast, that achieves a 50% reduction in cell infection at 1,295 μM , or SPC-14 with a binding affinity (KD) of 6.9 μM . Alternatively, active compounds show the presence of only up to two aromatic rings, attached to a more flexible backbone, as observed with LA, retinoids and vitamin K. Either group is predicted to have the ability to accommodate in the pocket, making different non-bonded interactions. Particularly, the presence of aromatic rings is likely essential so that π interactions can be established with the numerous phenylalanine residues, buried and spread across the pocket. Scaffolds capable of interacting with other hydrophobic amino acids that coat the deeper portions of the site are also favoured, as is the case of retinoids.

Regarding the hydrophilic entrance of the pocket, polar interactions with the amino acid residues present in this portion are common for stability, as initially identified with the co-crystallized LA. The carboxylic acid group appears to be an important feature to interact with the hydrophilic residues, but other functionalities, such as the sulfoxide in lifitegrast, also show the potential to make direct contacts with electrophilic residues in the vicinity. On the other hand, co-crystallized SPC-14 is buried in the pocket and unable to directly interact with these residues. The same behaviour is predicted for dexamethasone ¹⁹. Dexamethasone and SPC-14 have the lowest predicted LogP values (2.14 and 1.29, respectively), along with low logD values (-0.7 and 1.7, respectively), which may lead to an interaction pattern more dependent on the hydrophobic residues lining the deeper portions of the pocket, further away from the hydrophilic residues in the entrance. Considering the active compounds highlighted in this review, their chemical variety appears to be quite limited, as many studies focused on compounds similar to LA. However, the activity observed for lifitegrast indicates that more complex chemical scaffolds could possibly be associated with an improved overall occupation of the FABP, as can also be observed for SPC-14, with a new interaction pattern, similar to what previously predicted for dexamethasone ¹⁹. Further studies, such as the resolution of a three-dimensional structure of the FABP in complex with lifitegrast or dexamethasone, are needed to further confirm interactions leading to increased activity, and to elucidate if dexamethasone achieves the high activity observed with a pattern similar to SPC-14. Additionally, biological assays for SPC-14 are required to clarify if it is also capable of affecting the S-ACE2 interaction or the virus life cycle. The studies considered in this review, describing compounds identified as FABP ligands, can help to understand important features for FABP binding, and how this pocket can be explored to design optimized ligands. The chemical space of possible candidates has been significantly expanded since the first ligand

was identified, with the identification of bulkier scaffolds and new functional groups with biochemical and antiviral activity.

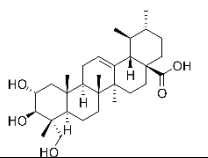
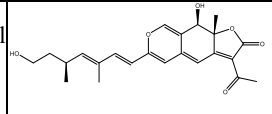
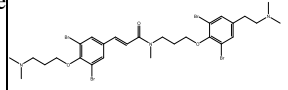
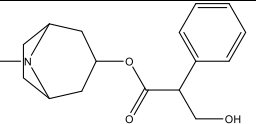
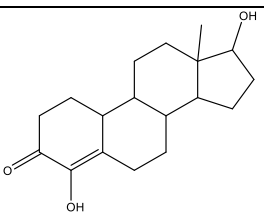
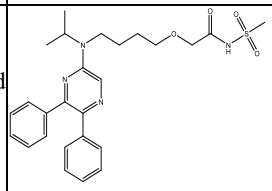
4.4 Compounds predicted to bind the FABP without reported experimental activity

Although experimental data is essential to validate virtual screening studies, this is not always available in published works describing virtual screening campaigns⁵⁴⁻⁵⁶, representing a significant limitation, as potential antiviral compounds cannot be selected for optimization before experimental confirmation⁵⁷. For example, as discussed previously, vitamin D and palmitic acid were both predicted to bind the FABP, but S-ACE2 binding inhibition assays proved otherwise^{30, 58}.

Since experimental results are an essential requirement to validate potential ligands in virtual screening studies, a clear separation is needed from the compounds shown in Table 1.

Although lacking experimental confirmation, the compounds listed in Table 2 have been predicted to bind to some residues in the FABP, based on their potential interactions in virtual screening studies. These compounds were selected considering the most common interaction features identified for confirmed ligands, namely hydrophobic contacts with phenylalanine residues that coat the pocket, or polar contacts with the hydrophilic amino acids Arg408, Gly408 and Lys417. Virtual screening methodologies are applied for compound libraries using a wide variety of targets and structures, from portions of the S protein (closed and open states, as well as pre- and post-fusion structures) to other SARS-CoV-2 proteins, such as the main protease or nucleocapsid protein⁵⁹.

Table 2 – Reported compounds with potential activity without validation in experimental assays

Compound	Total library	Structure	Interacting amino acids	cLogP ^a	LogD (pH=7) ^b	Molecular Weight	Reference
Asiatic acid	27 plant metabolites		Phe338, Tyr365, Leu368, Leu387, Phe392, Val395, Leu513, Val524	4.4	2.0	488.7	60
Rotiorinol C	92 natural compounds		Cys336, Phe338, Ala363, Phe374	2.6	1.2	398.4	59
Psammaphysene D	14 Marine Brominated Tyrosine Alkaloids		Gly339, Asn343, Ala344, Asp364, Ser366, Val367, Ser373, Phe374, Leu441, Arg509	6.6	0.9	783.24	61
Hyosciamine	92 natural compounds		Thr376, Val407, Ala411, Val433, Tyr508	1.8	-0.6	289.4	59
Oxabolone	11,875 approved drugs		No data reported	2.75	2.5	290.4	62
Selexipag	2456 approved drugs		Leu368, Phe374, Pro384, Asn388, Asp405, Gln409, Arg408, Lys417	3.25	2.84	496.6	63

^a Calculated with SwissADME ⁴⁸

^b Calculated using Chemaxon® LogD calculator ⁴⁹

Asiatic acid was included in a virtual screening study against the S glycoprotein, where multiple predicted residues described for interaction are also residues present in the FABP, such as Phe338, Tyr365 and Phe392⁶⁰. Additionally, asiatic acid is a pentacyclic triterpenoid, with a backbone similar to bile acid derivatives or dexamethasone, and it could therefore also bind to the pocket. Interactions with hydrophilic residues are not described, but multiple heteroatoms (belonging to carbonyl and hydroxyl groups) could potentially establish these interactions. A docking simulation was run to predict how asiatic acid may bind the FABP, and to assess if it has a similar behaviour to other sterols. However, no favourable binding poses could be obtained for this compound using Glide SP, potentially indicating an inefficient interaction with the FABP.⁴⁰ Likewise, although Psammaplysene D has been described to interact with some FABP residues (Ser373, Phe374), no favourable binding poses could be obtained using the Glide SP docking tool⁴⁰. In the case of Psammaplysene D, the failure to obtain docking poses could be due to the larger size of the molecule, with a molecular weight of 783.2 g/mol, significantly surpassing confirmed ligands and likely not fitting the pocket properly. As for asiatic acid, taking into account the binding predicted for dexamethasone and bile acid derivatives, the absence of docking poses obtained is unexpected. This lack of favourable binding poses could be due to the additional ring, as it has a pentacyclic structure, or to the lack of a carbon chain capable of interacting with the electrophilic pocket entrance, extending from the main ring system, as observed in both dexamethasone and the bile acid derivatives.

Rotiorinol C was also identified in a virtual screening study not directed at the FABP, when screened against the RBD portion of S protein (PDB ID: 6M17)⁵⁹. Several predicted interacting residues described in this study are in the FABP, particularly in the hydrophobic portion (Cys336, Phe338, Ser373 (H-bond), Phe374)⁵⁹. From a chemical point of view, rotiorinol C is similar to the retinoid backbone, with a flexible carbon chain and a rigid,

condensed ring system, suggesting potential activity due to FABP binding. The predicted binding pose obtained for rotiorinol C with molecular docking software Glide SP (Figure 15)⁴⁰ indicates extensive potential interactions in the FABP.

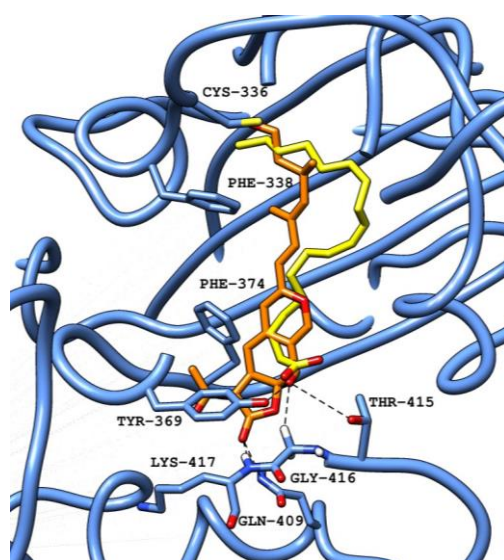


Figure 15: Crystallized LA (PDB ID: 6ZB5) (carbon atoms in yellow) superimposed with rotiorinol C (carbons atoms in orange) in the FABP in ribbon representation (blue). Black dashed lines represent polar interactions (hydrogen bonds and electrostatic interactions) between the ligand and amino acid residues in the protein⁵².

The main contacts are predicted with residues Gln409 and Lys417, Tyr369 and Gly416, with additional predicted interactions with Phe374 and Phe338, as initially identified. Extra interactions with Cys336 and Thr415 could further stabilize the molecule. When compared to other known ligands, occupation of the pocket is similar to lifitegrast, with logP (lifitegrast: 4.19, rotiorinol C: 2.6) and LogD (lifitegrast: 1.2, rotiorinol C: 1.2), as well as molecular weight (lifitegrast: 615.5, rotiorinol C: 398.4) compatible with binding to the FABP and subsequent potential effects for the inhibition of the S-ACE2 interaction.

Similarly, to rotiorinol C, hyosciamine was also identified in a virtual screening study not directed at the FABP, against multiple S protein conformations⁵⁹. Despite only a few

interacting residues highlighted in the FABP, a docking pose was generated for this compound using Glide SP (Figure 16)⁴⁰. This molecule has unique features when compared with the others discussed above, as it is more compact and contains a tropane ring that could further extend the chemical space of potential binders to this site and explore new potential interactions that may strengthen binding.

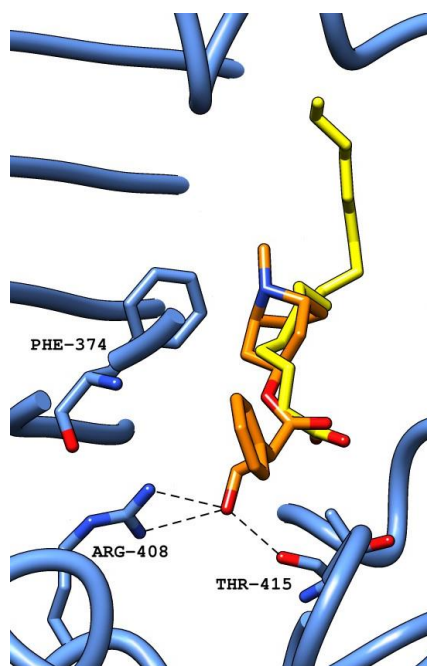


Figure 16: Crystallized LA (PDB ID: 6ZB5) (carbon atoms in yellow) superimposed with hyoscyamine (carbon atoms in orange) in the FABP in ribbon representation (blue). Black dashed lines represent polar interactions (hydrogen bonds and electrostatic interactions) between the ligand and amino acid residues in the protein⁵².

Due to the compact structure of hyoscyamine, the predicted binding pose in the FABP is characterised by limited pocket occupation, although some stabilizing interactions, particularly two H-bonds with Arg408 and Thr415 and an additional contact with Phe374, are predicted. Further experimental assays are needed to elucidate if hyoscyamine has any inhibitory activity of the S-ACE2 binding.

Oxabolone and Selexipag have been identified in two separate virtual screening studies directed at the FABP, based on the LA co-crystallized structure (PDB ID:6ZB5 and 6ZB4), and libraries of approved drugs^{62, 63}. However, none of these studies assessed biological activity or determined binding affinities with the S protein, therefore they still require validation for the virtual screening campaigns performed. As expected, the reported predicted binding and pocket occupation follows patterns previously identified, with oxabolone predicted to interact as SPC-14, whereas selexipag contains three aromatic rings and a flexible chain that extends towards the hydrophilic residues in the pocket^{62, 63}.

In summary, six additional compounds were identified as potential ligands to the FABP, based on their predicted interactions with the S protein, described in the original virtual screening studies that explored these chemical entities. Upon analysis of these molecules for their binding to the FABP using a molecular docking procedure, only for two of these potential ligands, rotiorinol C and hyoscyamine, favourable binding poses to this site could be observed. The binding pattern predicted for these two additional compounds is similar to what previously observed for confirmed ligands. Moreover, the molecular scaffold of rotiorinol C shares similar features with retinoids, as it shows the presence of a ring system attached to a carbon chain that contains a heteroatom, available to interact with the hydrophilic portion of the pocket. However, only experimental validation of the predicted activity may confirm the accuracy of these observations. Similarly, selexipag and oxabolone are predicted to interact with the FABP, but only experimental studies can validate the potential ability to affect the S-ACE2 interaction. On the other hand, hyoscyamine presents a novel chemical scaffold, featuring a tropane ring. Although its predicted pocket occupation appears limited compared to the confirmed active compounds, the experimental validation of its activity may open new avenues for the design of new therapeutic agents with diverse structural features.

5 Conclusions

The FABP in the S surface glycoprotein is a promising target for drug discovery for SARS-CoV-2: compounds binding to this site have the potential to exert a strong effect in cell recognition and cell infection, stabilizing the inactive conformation of the S glycoprotein.

The first known ligand for this pocket, LA, is capable of significantly affecting the virus-host interaction and cell infection. Identifying new, more potent binders to this site can provide the basis to develop novel, broad-spectrum treatment options against current and future-emerging coronaviruses.

In this review, we selected 20 studies, which describe 21 ligands with a confirmed binding and/or effect on the S-ACE2 interaction, and five additional ligands with a predicted binding to the FABP, for which no experimental results have been reported yet.

In addition to LA, lifitegrast has also been confirmed not only to have a strong inhibitory effect on the S-ACE2 interaction and ability to reduce cell infection, but also to directly bind to this pocket, showing that long, flexible carbon chains typical of fatty acids are not an essential requirement for binding. The confirmation of SPC-14 as a new binder, further indicates that different chemical scaffolds and interaction patterns can be accommodated in the pocket, although SPC-14 is still lacking experimental validation of inhibitory effect of Spike-ACE2 interaction or antiviral cell-based assays.

Since the remaining compounds discussed are predicted to bind the pocket and have either confirmed inhibitory activity of the S-ACE2 interaction or antiviral activity, with a reduction of cell infection in cell-based assays, their observed activity is likely due to binding to the FABP. Among the compounds with inhibitory or antiviral activity, multiple ring systems, such as the sterol backbone, are a recurring feature, with retinoids, such as tretinoin, and unsaturated fatty acids with long carbon chains also affecting the virus-host interaction. The

pattern of interactions is consistent, with common interactions established not only with the hydrophilic portion of the site, but critically throughout the hydrophobic region.

Additional compounds from virtual screening campaigns for which no experimental data is currently available have been analysed with docking simulations in the FABP. Among them, rotiorinol C is associated with the best predicted binding profile, indicating a likely potential for this molecule to affect the virus-host interaction.

Overall, the observations summarised in this review may enable the design of more potent, broad-spectrum new compounds, able to strongly bind the FABP and therefore prevent cell recognition and entry of coronaviruses currently affecting humans, and of those possibly emerging in the future.

6 Data and Software Availability

Not Applicable

7 Funding

L.Q.-R. would like to acknowledge Fundação para a Ciência e para a Tecnologia for the grant “2020.10230.BD” under the program “DOCTORATES 4 COVID-19” and EEA Grants/Norway Grants for the grant “FBR_OC52_53”.

8 Supporting information

Supporting Information contains PRISMA diagram for inclusion of studies and chemical structures of all compounds reported (as SMILES). This material is available free of charge via the Internet at <http://pubs.acs.org>.

9 References

- (1) Wang, M. Y.; Zhao, R.; Gao, L. J.; Gao, X. F.; Wang, D. P.; Cao, J. M. SARS-CoV-2: Structure, Biology, and Structure-Based Therapeutics Development. *Front Cell Infect Microbiol* **2020**, *10*, 587269. DOI: 10.3389/fcimb.2020.587269 From NLM.
- (2) WHO Director-General's opening remarks at the media briefing on COVID-19 - 11 March 2020. 2020. (accessed 09/03/2021).
- (3) WHO. Coronavirus Disease (COVID-19) Dashboard. WHO 2020. <https://covid19.who.int/> (accessed 2023/09/04).
- (4) Hu, B.; Guo, H.; Zhou, P.; Shi, Z. L. Characteristics of SARS-CoV-2 and COVID-19. *Nat Rev Microbiol* **2021**, *19* (3), 141-154. DOI: 10.1038/s41579-020-00459-7 From NLM.
- (5) Woo, P. C.; Lau, S. K.; Huang, Y.; Yuen, K. Y. Coronavirus diversity, phylogeny and interspecies jumping. *Exp Biol Med (Maywood)* **2009**, *234* (10), 1117-1127. DOI: 10.3181/0903-mr-94 From NLM.
- (6) Schoeman, D.; Gordon, B.; Fielding, B. C. Pathogenic Human Coronaviruses. *Reference Module in Biomedical Sciences* **2021**, B978-970-912-818731-818739.800052-818735. DOI: 10.1016/B978-0-12-818731-9.00052-5 PMC.
- (7) Wrapp, D.; Wang, N.; Corbett, K. S.; Goldsmith, J. A.; Hsieh, C.-L.; Abiona, O.; Graham, B. S.; McLellan, J. S. Cryo-EM structure of the 2019-nCoV spike in the prefusion conformation. *Science* **2020**, *367* (6483), 1260-1263. DOI: 10.1126/science.abb2507.
- (8) Walls, A. C.; Park, Y. J.; Tortorici, M. A.; Wall, A.; McGuire, A. T.; Velesler, D. Structure, Function, and Antigenicity of the SARS-CoV-2 Spike Glycoprotein. *Cell* **2020**, *181* (2), 281-292.e286. DOI: 10.1016/j.cell.2020.02.058 From NLM.
- (9) Huang, Y.; Yang, C.; Xu, X.-f.; Xu, W.; Liu, S.-w. Structural and functional properties of SARS-CoV-2 spike protein: potential antivirus drug development for COVID-19. *Acta Pharmacologica Sinica* **2020**, *41* (9), 1141-1149. DOI: 10.1038/s41401-020-0485-4.
- (10) Queirós-Reis, L.; Gomes da Silva, P.; Gonçalves, J.; Brancale, A.; Bassetto, M.; Mesquita, J. R. SARS-CoV-2 Virus-Host Interaction: Currently Available Structures and Implications of Variant Emergence on Infectivity and Immune Response. *International Journal of Molecular Sciences* **2021**, *22* (19), 10836.

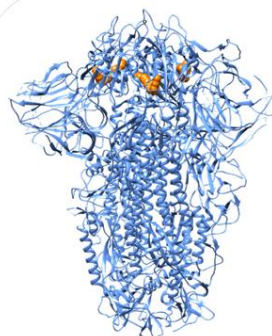
- (11) Xia, X. Domains and Functions of Spike Protein in Sars-Cov-2 in the Context of Vaccine Design. *Viruses* **2021**, *13* (1). DOI: 10.3390/v13010109 From NLM.
- (12) Shang, J.; Ye, G.; Shi, K.; Wan, Y.; Luo, C.; Aihara, H.; Geng, Q.; Auerbach, A.; Li, F. Structural basis of receptor recognition by SARS-CoV-2. *Nature* **2020**, *581* (7807), 221-224. DOI: 10.1038/s41586-020-2179-y.
- (13) Chemical Computing Group, I. *Molecular Operating Environment (MOE 2019.10)*. Chemical Computing Group, Inc., <http://www.chemcomp.com> (accessed 2023/05/07)
- (14) Vogel, A. B.; Kanevsky, I.; Che, Y.; Swanson, K. A.; Muik, A.; Vormehr, M.; Kranz, L. M.; Walzer, K. C.; Hein, S.; Güler, A.; et al. BNT162b vaccines protect rhesus macaques from SARS-CoV-2. *Nature* **2021**. DOI: 10.1038/s41586-021-03275-y.
- (15) Sinha, S. K.; Shakya, A.; Prasad, S. K.; Singh, S.; Gurav, N. S.; Prasad, R. S.; Gurav, S. S. An in-silico evaluation of different Saikosaponins for their potency against SARS-CoV-2 using NSP15 and fusion spike glycoprotein as targets. *J Biomol Struct Dyn* **2021**, *39* (9), 3244-3255. DOI: 10.1080/07391102.2020.1762741 From NLM.
- (16) Romeo, A.; Iacovelli, F.; Falconi, M. Targeting the SARS-CoV-2 spike glycoprotein prefusion conformation: virtual screening and molecular dynamics simulations applied to the identification of potential fusion inhibitors. *Virus Res* **2020**, *286*, 198068. DOI: 10.1016/j.virusres.2020.198068 From NLM.
- (17) Rodríguez, Y.; Cardoze, S. M.; Obineche, O. W.; Melo, C.; Persaud, A.; Fernández Romero, J. A. Small Molecules Targeting SARS-CoV-2 Spike Glycoprotein Receptor-Binding Domain. *ACS Omega* **2022**, *7* (33), 28779-28789. DOI: 10.1021/acsomega.2c00844.
- (18) Chan, W. K. B.; Olson, K. M.; Wotring, J. W.; Sexton, J. Z.; Carlson, H. A.; Traynor, J. R. In silico analysis of SARS-CoV-2 proteins as targets for clinically available drugs. *Scientific Reports* **2022**, *12* (1), 5320. DOI: 10.1038/s41598-022-08320-y.
- (19) Shoemark, D. K.; Colenso, C. K.; Toelzer, C.; Gupta, K.; Sessions, R. B.; Davidson, A. D.; Berger, I.; Schaffitzel, C.; Spencer, J.; Mulholland, A. J. Molecular Simulations suggest Vitamins, Retinoids and Steroids as Ligands of the Free Fatty Acid Pocket of the SARS-CoV-2 Spike Protein*. *Angew Chem Int Ed Engl* **2021**, *60* (13), 7098-7110. DOI: 10.1002/anie.202015639 From NLM.
- (20) Mohebbi, A.; Askari, F. S.; Sammak, A. S.; Ebrahimi, M.; Najafimemar, Z. Druggability of cavity pockets within SARS-CoV-2 spike glycoprotein and pharmacophore-based drug discovery. *Future Virology* **2021**, *16* (6), 389-397. DOI: 10.2217/fvl-2020-0394.
- (21) Siragusa, L.; Menna, G.; Buratta, F.; Baroni, M.; Desantis, J.; Cruciani, G.; Goracci, L. CROMATIC: Cross-Relationship Map of Cavities from Coronaviruses. *Journal of Chemical Information and Modeling* **2022**, *62* (12), 2901-2908. DOI: 10.1021/acs.jcim.2c00169.
- (22) Ghosh, D.; Ghosh Dastidar, D.; Roy, K.; Ghosh, A.; Mukhopadhyay, D.; Sikdar, N.; Biswas, N. K.; Chakrabarti, G.; Das, A. Computational prediction of the molecular mechanism of statin group of drugs against SARS-CoV-2 pathogenesis. *Scientific Reports* **2022**, *12* (1), 6241. DOI: 10.1038/s41598-022-09845-y.
- (23) Yan, B.; Chu, H.; Yang, D.; Sze, K. H.; Lai, P. M.; Yuan, S.; Shuai, H.; Wang, Y.; Kao, R. Y.; Chan, J. F.; et al. Characterization of the Lipidomic Profile of Human Coronavirus-Infected Cells: Implications for Lipid Metabolism Remodeling upon Coronavirus Replication. *Viruses* **2019**, *11* (1). DOI: 10.3390/v11010073 From NLM.
- (24) Toelzer, C.; Gupta, K.; Yadav, S. K. N.; Borucu, U.; Davidson, A. D.; Kavanagh Williamson, M.; Shoemark, D. K.; Garzoni, F.; Staufer, O.; Milligan, R.; et al. Free fatty acid binding pocket in the locked structure of SARS-CoV-2 spike protein. *Science* **2020**, *370* (6517), 725-730. DOI: 10.1126/science.abd3255.
- (25) Toelzer, C.; Gupta, K.; Yadav, S. K. N.; Hodgson, L.; Williamson, M. K.; Buzas, D.; Borucu, U.; Powers, K.; Stenner, R.; Vasileiou, K.; et al. The free fatty acid binding pocket is a conserved hallmark in pathogenic coronavirus spike proteins from SARS-CoV to Omicron. *Science Advances* **2022**, *8* (47), eadc9179. DOI: doi:10.1126/sciadv.adc9179.

- (26) Xu, C.; Wang, Y.; Liu, C.; Zhang, C.; Han, W.; Hong, X.; Wang, Y.; Hong, Q.; Wang, S.; Zhao, Q.; et al. Conformational dynamics of SARS-CoV-2 trimeric spike glycoprotein in complex with receptor ACE2 revealed by cryo-EM. *Sci Adv* **2021**, *7* (1). DOI: 10.1126/sciadv.abe5575 From NLM.
- (27) Ke, Z.; Oton, J.; Qu, K.; Cortese, M.; Zila, V.; McKeane, L.; Nakane, T.; Zivanov, J.; Neufeldt, C. J.; Cerikan, B.; et al. Structures and distributions of SARS-CoV-2 spike proteins on intact virions. *Nature* **2020**, *588* (7838), 498-502. DOI: 10.1038/s41586-020-2665-2.
- (28) Benton, D. J.; Wrobel, A. G.; Roustan, C.; Borg, A.; Xu, P.; Martin, S. R.; Rosenthal, P. B.; Skehel, J. J.; Gamblin, S. J. The effect of the D614G substitution on the structure of the spike glycoprotein of SARS-CoV-2. *Proceedings of the National Academy of Sciences* **2021**, *118* (9), e2022586118. DOI: doi:10.1073/pnas.2022586118.
- (29) Stauffer, O.; Gupta, K.; Hernandez Bücher, J. E.; Kohler, F.; Sigl, C.; Singh, G.; Vasileiou, K.; Yagüe Relimpio, A.; Macher, M.; Fabritz, S.; et al. Synthetic virions reveal fatty acid-coupled adaptive immunogenicity of SARS-CoV-2 spike glycoprotein. *Nature Communications* **2022**, *13* (1), 868. DOI: 10.1038/s41467-022-28446-x.
- (30) Goc, A.; Niedzwiecki, A.; Rath, M. Polyunsaturated ω -3 fatty acids inhibit ACE2-controlled SARS-CoV-2 binding and cellular entry. *Scientific Reports* **2021**, *11* (1), 5207. DOI: 10.1038/s41598-021-84850-1.
- (31) Fonnesu, R.; Thunuguntla, V.; Veeramachaneni, G. K.; Bondili, J. S.; La Rocca, V.; Filipponi, C.; Spezia, P. G.; Sidoti, M.; Plicanti, E.; Quaranta, P.; et al. Palmitoylethanolamide (PEA) Inhibits SARS-CoV-2 Entry by Interacting with S Protein and ACE-2 Receptor. *Viruses* **2022**, *14* (5). DOI: 10.3390/v14051080 From NLM.
- (32) Vivar-Sierra, A.; Araiza-Macías, M. J.; Hernández-Contreras, J. P.; Vergara-Castañeda, A.; Ramírez-Vélez, G.; Pinto-Almazán, R.; Salazar, J. R.; Loza-Mejía, M. A. In Silico Study of Polyunsaturated Fatty Acids as Potential SARS-CoV-2 Spike Protein Closed Conformation Stabilizers: Epidemiological and Computational Approaches. *Molecules* **2021**, *26* (3), 711.
- (33) Sofia, F. O. A.; Shoemark, D. K.; Avila Ibarra, A.; Davidson, A. D.; Berger, I.; Schaffitzel, C.; Mulholland, A. J. The fatty acid site is coupled to functional motifs in the SARS-CoV-2 spike protein and modulates spike allosteric behaviour. *Comput Struct Biotechnol J* **2022**, *20*, 139-147. DOI: 10.1016/j.csbj.2021.12.011 From NLM.
- (34) Warwicker, J. A model for pH coupling of the SARS-CoV-2 spike protein open/closed equilibrium. *Brief Bioinform* **2021**, *22* (2), 1499-1507. DOI: 10.1093/bib/bbab056 From NLM.
- (35) Yurkovetskiy, L.; Wang, X.; Pascal, K. E.; Tomkins-Tinch, C.; Nyalile, T.; Wang, Y.; Baum, A.; Diehl, W. E.; Dauphin, A.; Carbone, C.; et al. SARS-CoV-2 Spike protein variant D614G increases infectivity and retains sensitivity to antibodies that target the receptor binding domain. *bioRxiv* **2020**. DOI: 10.1101/2020.07.04.187757 From NLM.
- (36) Zhou, T.; Tsybovsky, Y.; Gorman, J.; Rapp, M.; Cerutti, G.; Chuang, G.-Y.; Katsamba, P. S.; Sampson, J. M.; Schön, A.; Bimela, J.; et al. Cryo-EM Structures of SARS-CoV-2 Spike without and with ACE2 Reveal a pH-Dependent Switch to Mediate Endosomal Positioning of Receptor-Binding Domains. *Cell Host & Microbe* **2020**, *28* (6), 867-879.e865. DOI: <https://doi.org/10.1016/j.chom.2020.11.004>.
- (37) Kadam, S. B.; Sukhramani, G. S.; Bishnoi, P.; Pable, A. A.; Barvkar, V. T. SARS-CoV-2, the pandemic coronavirus: Molecular and structural insights. *J Basic Microbiol* **2021**. DOI: 10.1002/jobm.202000537 From NLM.
- (38) Ma, J.; Su, D.; Sun, Y.; Huang, X.; Liang, Y.; Fang, L.; Ma, Y.; Li, W.; Liang, P.; Zheng, S. Cryo-electron Microscopy Structure of S-Trimer, a Subunit Vaccine Candidate for COVID-19. *Journal of Virology* **2021**, *95* (11), e00194-00121. DOI: doi:10.1128/JVI.00194-21.
- (39) Preferred reporting items for systematic review and meta-analysis protocols (PRISMA-P) 2015: elaboration and explanation. *BMJ* **2016**, *354*, i4086. DOI: 10.1136/bmj.i4086.
- (40) Schrödinger. Release 2020-4: Glide. Schrödinger, LLC New York, NY, USA: 2020.
- (41) Balunas, M. J.; Kinghorn, A. D. Drug discovery from medicinal plants. *Life Sciences* **2005**, *78* (5), 431-441. DOI: <https://doi.org/10.1016/j.lfs.2005.09.012>.

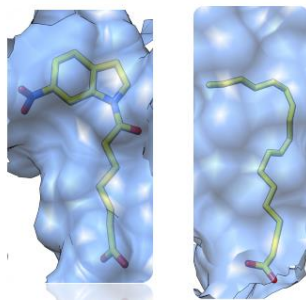
- (42) Carino, A.; Moraca, F.; Fiorillo, B.; Marchianò, S.; Sepe, V.; Biagioli, M.; Finamore, C.; Bozza, S.; Francisci, D.; Distrutti, E.; et al. Hijacking SARS-CoV-2/ACE2 Receptor Interaction by Natural and Semi-synthetic Steroidal Agents Acting on Functional Pockets on the Receptor Binding Domain. *Frontiers in Chemistry* **2020**, *8*, Original Research. DOI: 10.3389/fchem.2020.572885.
- (43) Riva, L.; Yuan, S.; Yin, X.; Martin-Sancho, L.; Matsunaga, N.; Pache, L.; Burgstaller-Muehlbacher, S.; De Jesus, P. D.; Teriete, P.; Hull, M. V.; et al. Discovery of SARS-CoV-2 antiviral drugs through large-scale compound repurposing. *Nature* **2020**, *586* (7827), 113-119. DOI: 10.1038/s41586-020-2577-1 From NLM.
- (44) Sharanya, C. S.; Sabu, A.; Haridas, M. Potent phytochemicals against COVID-19 infection from phyto-materials used as antivirals in complementary medicines: a review. *Future Journal of Pharmaceutical Sciences* **2021**, *7* (1), 113. DOI: 10.1186/s43094-021-00259-7.
- (45) Creutzmacher, R.; Maass, T.; Veselkova, B.; Ssebyatika, G.; Krey, T.; Empting, M.; Tautz, N.; Frank, M.; Kölbel, K.; Uetrecht, C.; et al. NMR Experiments Provide Insights into Ligand-Binding to the SARS-CoV-2 Spike Protein Receptor-Binding Domain. *Journal of the American Chemical Society* **2022**, *144* (29), 13060-13065. DOI: 10.1021/jacs.2c05603.
- (46) Day, C. J.; Bailly, B.; Guillon, P.; Dirr, L.; Jen, F. E.-C.; Spillings, B. L.; Mak, J.; Itzstein, M. v.; Haselhorst, T.; Jennings, M. P. Multidisciplinary Approaches Identify Compounds that Bind to Human ACE2 or SARS-CoV-2 Spike Protein as Candidates to Block SARS-CoV-2–ACE2 Receptor Interactions. *mBio* **2021**, *12* (2), e03681-03620. DOI: doi:10.1128/mBio.03681-20.
- (47) Wang, Q.; Meng, F.; Xie, Y.; Wang, W.; Meng, Y.; Li, L.; Liu, T.; Qi, J.; Ni, X.; Zheng, S.; et al. In Silico Discovery of Small Molecule Modulators Targeting the Achilles' Heel of SARS-CoV-2 Spike Protein. *ACS Cent Sci* **2023**, *9* (2), 252-265. DOI: 10.1021/acscentsci.2c01190 From NLM.
- (48) Daina, A.; Michielin, O.; Zoete, V. SwissADME: a free web tool to evaluate pharmacokinetics, drug-likeness and medicinal chemistry friendliness of small molecules. *Scientific Reports* **2017**, *7* (1), 42717. DOI: 10.1038/srep42717.
- (49) *LogD Predictor*; 2023. (accessed).
- (50) Haber, S. L.; Benson, V.; Buckway, C. J.; Gonzales, J. M.; Romanet, D.; Scholes, B. Lifitegrast: a novel drug for patients with dry eye disease. *Ther Adv Ophthalmol* **2019**, *11*, 2515841419870366. DOI: 10.1177/2515841419870366 From NLM.
- (51) Friesner, R. A.; Banks, J. L.; Murphy, R. B.; Halgren, T. A.; Klicic, J. J.; Mainz, D. T.; Repasky, M. P.; Knoll, E. H.; Shelley, M.; Perry, J. K.; et al. Glide: A New Approach for Rapid, Accurate Docking and Scoring. 1. Method and Assessment of Docking Accuracy. *Journal of Medicinal Chemistry* **2004**, *47* (7), 1739-1749. DOI: 10.1021/jm0306430.
- (52) Pettersen, E. F.; Goddard, T. D.; Huang, C. C.; Couch, G. S.; Greenblatt, D. M.; Meng, E. C.; Ferrin, T. E. UCSF Chimera--a visualization system for exploratory research and analysis. *J Comput Chem* **2004**, *25* (13), 1605-1612. DOI: 10.1002/jcc.20084 From NLM.
- (53) Le Guilloux, V.; Schmidtke, P.; Tuffery, P. Fpocket: An open source platform for ligand pocket detection. *BMC Bioinformatics* **2009**, *10* (1), 168. DOI: 10.1186/1471-2105-10-168.
- (54) Gimeno, A.; Ojeda-Montes, M. J.; Tomás-Hernández, S.; Cereto-Massagué, A.; Beltrán-Debón, R.; Mulero, M.; Pujadas, G.; Garcia-Vallvé, S. The Light and Dark Sides of Virtual Screening: What Is There to Know? *Int J Mol Sci* **2019**, *20* (6). DOI: 10.3390/ijms20061375 From NLM.
- (55) Zhu, T.; Cao, S.; Su, P. C.; Patel, R.; Shah, D.; Chokshi, H. B.; Szukala, R.; Johnson, M. E.; Hevener, K. E. Hit identification and optimization in virtual screening: practical recommendations based on a critical literature analysis. *J Med Chem* **2013**, *56* (17), 6560-6572. DOI: 10.1021/jm301916b From NLM.
- (56) Durrant, J. D.; McCammon, J. A. NNScore 2.0: A Neural-Network Receptor–Ligand Scoring Function. *Journal of Chemical Information and Modeling* **2011**, *51* (11), 2897-2903. DOI: 10.1021/ci2003889.
- (57) Kolb, P.; Ferreira, R. S.; Irwin, J. J.; Shoichet, B. K. Docking and chemoinformatic screens for new ligands and targets. *Current Opinion in Biotechnology* **2009**, *20* (4), 429-436. DOI: <https://doi.org/10.1016/j.copbio.2009.08.003>.

- (58) Bender, B. J.; Gahbauer, S.; Lutten, A.; Lyu, J.; Webb, C. M.; Stein, R. M.; Fink, E. A.; Balias, T. E.; Carlsson, J.; Irwin, J. J.; et al. A practical guide to large-scale docking. *Nature Protocols* **2021**, *16* (10), 4799-4832. DOI: 10.1038/s41596-021-00597-z.
- (59) Skariyachan, S.; Gopal, D.; Muddebihalkar, A. G.; Uttarkar, A.; Niranjana, V. Structural insights on the interaction potential of natural leads against major protein targets of SARS-CoV-2: Molecular modelling, docking and dynamic simulation studies. *Comput Biol Med* **2021**, *132*, 104325. DOI: 10.1016/j.compbiomed.2021.104325 From NLM.
- (60) Azim, K. F.; Ahmed, S. R.; Banik, A.; Khan, M. M. R.; Deb, A.; Somana, S. R. Screening and druggability analysis of some plant metabolites against SARS-CoV-2: An integrative computational approach. *Informatics in Medicine Unlocked* **2020**, *20*, 100367. DOI: <https://doi.org/10.1016/j.imu.2020.100367>.
- (61) El-Demerdash, A.; Hassan, A.; Abd El-Aziz, T. M.; Stockand, J. D.; Arafa, R. K. Marine Brominated Tyrosine Alkaloids as Promising Inhibitors of SARS-CoV-2. *Molecules* **2021**, *26* (20), 6171.
- (62) Piplani, S.; Singh, P.; Petrovsky, N.; Winkler, D. A. Identifying SARS-CoV-2 Drugs Binding to the Spike Fatty Acid Binding Pocket Using In Silico Docking and Molecular Dynamics. *Int J Mol Sci* **2023**, *24* (4). DOI: 10.3390/ijms24044192 From NLM.
- (63) Prajapat, M.; Sarma, P.; Shekhar, N.; Chauhan, A.; Kaur, G.; Bhattacharyya, A.; Avti, P.; Choudhary, G.; Bansal, S.; Sharma, S.; et al. Virtual screening and molecular dynamics simulation study of approved drugs as a binder to the linoleic acid binding site on spike protein of SARS-CoV-2 and double mutant (E484Q and L452R). *Indian J Pharmacol* **2022**, *54* (6), 431-442. DOI: 10.4103/ijp.ijp_111_22 From NLM.

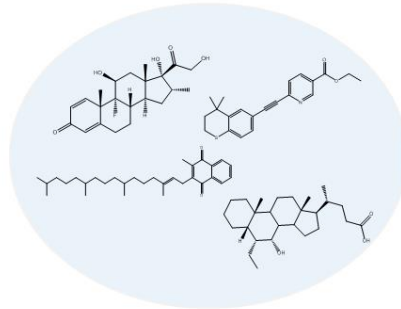
Systematic review of literature → 738 identified manuscripts



SARS-CoV-2 Spike protein
Fatty Acid Binding Pocket
(FABP)



Confirmed ligands of FABP



Potential ligands with inhibitory activity



Foundation for the design of new ligands with antiviral activity